Title

Angle-resolved nonresonant two-photon single ionization of argon using 9.3-eV photons produced via high-order harmonic generation

Journal

Physical Review A, 101(6)

ISSN

2469-9926

Authors

Larsen, Kirk A

Slaughter, Daniel S

Weber, Thorsten

Publication Date

2020-06-01

DOI

10.1103/physreva.101.061402

Peer reviewed

Angle-resolved nonresonant two-photon single ionization of argon using 9.3-eV photons produced via high-order harmonic generation

Kirk A. Larsen,[1,2,*] Daniel S. Slaughter,[2] and Thorsten Weber[2]
[1]*Graduate Group in Applied Science and Technology, University of California, Berkeley, California 94720, USA*
[2]*Chemical Sciences Division, Lawrence Berkeley National Laboratory, Berkeley, California 94720, USA*

We present an experimental study on the photoionization dynamics of nonresonant one-color two-photon single valence ionization of neutral argon atoms. Using 9.3-eV photons produced via high harmonic generation and a three-dimensional momentum imaging spectrometer, we detect the photoelectrons and ions produced from nonresonant two-photon ionization in coincidence. Photoionization from the $3p$ orbital produces a photoelectron scattering wave function with p- and f-partial-wave components, which interfere and result in a photoelectron angular distribution with peak amplitude perpendicular to the vacuum ultraviolet polarization. The comparison between the present results and the two previous sets of theoretical calculations [Phys. Rev. A **44**, 324 (1991), and J. Phys. B: At. Mol. Phys. **16**, 2737 (1983)] indicates that electron-electron correlation contributes appreciably to the two-photon ionization dynamics.

The photoionization dynamics of multielectron atomic and molecular systems are influenced by electron-electron correlation. Nonresonant two-photon ionization can probe such correlation effects in both the initial and the final states of the target. A particularly sensitive observable is the photoelectron angular distribution (PAD), which can provide a detailed view of the underlying mechanisms involved in the photoionization process and its correlated nature, e.g., information on the role of continuum states and interchannel coupling [1–12]. The PAD emerges from a coherent summation over a set of final continuum states. The sensitivity of the PAD to electron-electron correlation arises from its dependence on the amplitudes and phases of the different partial-wave components of the coherent sum. These distinct angular momentum components can interfere to create nodes and antinodes in the PAD.

PADs are uniquely characterized by their energy-dependent anisotropy parameters or β parameters. The number of β terms used to describe the PAD increases with the photon order. As such, a two-photon PAD can exhibit more anisotropy and structure than the corresponding one-photon PAD. Previous two-photon investigations of the anisotropy parameters in neon and argon have been realized using two-color two-photon above-threshold ionization schemes [13–15] where ionization was performed with a vacuum ultraviolet (VUV) field in the presence of a strong NIR dressing field that generated photoelectron sidebands. This can make a comparison with theory very challenging. Measurements that lie within the perturbative limit and target nonresonant bound-continuum transitions, driven by the second photon (rather than continuum-continuum transitions), are highly sensitive to electron-electron correlation and can be achieved in a one-color two-photon ionization scheme by exclusively using a VUV field with a photon energy in a nonresonant region below the ionization threshold. However, measuring a PAD from Nonresonant One-color Two-Photon Single Ionization (NOTPSI) in an atomic gas requires sufficiently high VUV intensities to enable nonlinear processes. Since high intensity ultrashort VUV light sources are limited to a small number of free-electron lasers (FELs) and tabletop high-order harmonic generation (HHG) systems, angle-resolved measurements on NOTPSI in rare gases are scarce.

Over the years, several studies have investigated one-color two-photon ionization in rare gases, first using HHG-based light sources [16,17], and later using VUV FELs [18–20]. PADs were measured in helium at several photon energies across both the resonant and the nonresonant regions, in Ref. [20]. Here, anisotropy parameters as well as amplitude ratios and phase differences of the partial-wave components of the scattering wave function could be extracted due to the simple nature of the target. By moving to more complex many-electron systems, more terms and higher angular momentum components contribute to the photoelectron scattering wave function, and many-electron effects become more significant. This increase in complexity represents a great challenge for experiment and theory alike.

Previous theoretical studies on angle-resolved two-photon ionization in helium have indicated that a single-active-electron picture appears to be a valid approach in describing the photoionization dynamics for photon energies below the ionization threshold (and even in the above-threshold region) [1]. It is unlikely that this is true for more complex core targets. This compels angle-resolved measurements in more complicated systems where many active and correlated electrons are required to describe the photoionization dynamics. To our knowledge, no angle-resolved measurements exist for complex multielectron systems, such as argon where

*klarsen@lbl.gov

electron-electron correlation is expected to play a more significant role in the photoionization dynamics than in simple systems, such as helium. The aim of this experimental investigation is to reveal clear contributions from electron-electron correlation in the PADs emerging from NOTPSI of argon.

Despite the paucity of experimental data, the problem has not escaped theoretical treatment. Over a quarter of a century ago, the β parameters for one-color two-photon single ionization (including NOTPSI) were calculated for argon using a Hartree-Fock approach [21] providing uncorrelated, Coulomb correlated results, and a random-phase-approximation calculation [22], which neglected electron-electron correlation. The uncorrelated results of Refs. [21,22] are somewhat ambiguous due to discrepancies between the calculations performed in the length and velocity gauge at various photon energies. The correlated results of Ref. [21] show better gauge invariance in both the resonant and the nonresonant two-photon ionization regions, and the computed β parameters suggest maximum photoelectron emission perpendicular to the ionizing field at 9.3 eV. However, to our knowledge, these calculations have, for decades, remained unverified by any experimental measurement.

In this Rapid Communication, we present results on angle-resolved NOTPSI of argon from the $3p$ orbital using three-dimensional (3D) momentum imaging where the photoelectron and ion are measured in coincidence. Using a 400-nm driving field, we produce and select VUV photons with an energy of 9.3 eV via HHG, which are then used to perform NOTPSI. Interference between different angular momentum components of the photoelectron wave function results in a PAD exhibiting maximum intensity perpendicular to the ionizing VUV field. These experimental results are compared against previous calculations, which suggest that electron-electron correlation considerably influences the photoionization dynamics.

The valence photoionization dynamics in neutral argon were investigated using the COLd Target Recoil Ion Momentum Spectroscopy (COLTRIMS) [23–26] technique. Here, the photoelectron-ion pair produced by NOTPSI are collected with a full-4π solid angle, and their 3D momenta are measured in coincidence on an event-by-event basis. The charged particles are guided by parallel DC electric and magnetic fields (15.55 V/cm, 3.72 G) towards position- and time-sensitive detectors at opposite ends of the spectrometer. The detectors consist of a multichannel plate (MCP) chevron stack with a delay-line anode readout [27,28]. The electron and ion detectors are a three-layer hex anode with an 80-mm MCP and a two-layer quad anode with a 120-mm MCP, respectively. The 3D momentum of each charge carrier is encoded into its hit position on the detector and its time of flight relative to the laser trigger.

The laser system has been described previously [26], but we briefly highlight a few modifications made to the system below. A Ti:sapphire near-infrared (NIR) laser system produces 12-mJ 45-fs pulses at 50 Hz, which are frequency doubled using a 0.25-mm-thick β-barium borate crystal where the co-propagating 800-nm NIR and 400-nm blue fields are then separated using two dichroic mirrors. The reflected blue photons ($\sim$3.6 mJ, $\sim$50 fs) are focused ($f = 6$ m) into a 10-cm-long gas cell containing 3 Torr of krypton to generate VUV odd harmonics via HHG. The resulting VUV frequency comb is then separated from the 400-nm fundamental by reflection from three silicon mirrors near Brewster's angle for the 400-nm field, resulting in a suppression of the fundamental by a factor of $<10^{-6}$. The third harmonic (133 nm, 9.3 eV) is isolated by transmission through a 0.25-mm-thick MgF_2 window, which totally suppresses the fifth harmonic and above. The femtosecond pulse duration of the third harmonic is also maintained, whereas the residual 400-nm pulse is temporally separated from the third-harmonic pulse by $\sim$700 fs due to the difference in the group-velocity dispersion (GVD) of the window at ω_0 and $3\omega_0$ [29,30]. After transmission through the window, we estimate the pulse duration of the third harmonic to be $\sim$30 fs, based on its spectral bandwidth, its estimated attochirp, the thickness, and the GVD of the MgF_2 window [31,32]. The femtosecond 9.3-eV pulses are then backfocused ($f = 15$ cm) into the 3D momentum imaging spectrometer using a protected aluminum mirror, the reflectance of which has been measured to be 43% at 9.3 eV [33]. The pulse energy of the third harmonic on the target is approximately 10 nJ, which was measured using a pair of broadband VUV filters (Acton Optics FB130-B-1D.3) and a calibrated photodiode.

A beam of argon atoms is prepared from an adiabatic expansion through a 0.03-mm nozzle, which is then collimated by a pair of skimmers. This atomic jet propagates perpendicular to the focusing VUV beam where the two intersect in the interaction region (approximately $0.01 \times 0.01 \times 0.20$ mm^3) of the spectrometer, resulting in a NOTPSI rate of $\sim$0.3 events per VUV pulse.

The ground-state electronic configuration of argon is $1s^2\,2s^2\,2p^6\,3s^2\,3p^6$ (^{1}S). Ionization from the $3p$-orbital results in the ground electronic state of the cation Ar^+, a ^2P state. From two-photon selection rules, the final states must have either ^1S or ^1D total symmetry, whereas the photoelectron wave function must be either a p or an f wave. It follows that we can express the allowed final states in the three forms listed below:

$$^1S : 3p^5\ ^2P + \epsilon p, \tag{1}$$

$$^1D : 3p^5\ ^2P + \epsilon p, \tag{2}$$

$$^1D : 3p^5\ ^2P + \epsilon f. \tag{3}$$

In (2) and (3) above, we see that the ^1D final state contains contributions from two different photoelectron angular momentum components, p and f waves. The coherent sum of these two partial waves can create an interference pattern in the PAD. Since the initial state has total magnetic quantum number $M = 0$, so too must the final states. Hence, the m value of the photoelectron and ion wave functions must sum to 0. From this restriction, we see that only $m = 0, \pm 1$ values of the f-wave component can contribute, whereas all m values of the p waves may contribute. These photoelectron states are paired to states of the core with the appropriate m value.

A diagram depicting the NOTPSI pathway in the present experiment is shown in Fig. 1. The gray box indicates the region containing the bound excited states of argon beginning at 11.55 eV. The ionization potential of argon is 15.76 eV, whereas the two-photon energy is $\sim$18.6 eV, which results in an expected photoelectron kinetic energy of roughly 2.8 eV. Ionization of the ground-state atoms via nonresonant

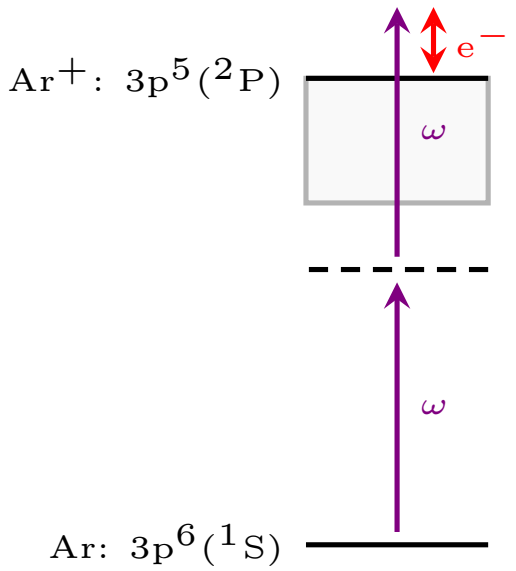

FIG. 1. An energy-level diagram depicting the NOTPSI pathway from the $3p$ orbital of Ar at 9.3 eV. The gray box indicates the region containing bound excited states, the first appearing at 11.55 eV. The ionization potential of Ar is 15.76 eV, hence, the red double arrow corresponds with a photoelectron kinetic energy of 2.84 eV.

two-photon absorption populates an ionic state and releases an electron into the continuum, with allowed final states listed in (1)–(3) above.

The measured photoelectron kinetic-energy spectrum is presented in Fig. 2(a). Here, we observe a single peak centered at 2.8 eV with a full width at half maximum of ∼400 meV, indicative of the two-photon spectral bandwidth of the third harmonic (convolved with the electron energy resolution of the spectrometer). The photoelectron momentum distribution transverse versus parallel to the VUV polarization vector is shown in Fig. 2(b) where we observe electron emission peaking towards high transverse momentum and low longitudinal momentum. To gain more insight into the photoelectron emission pattern, we turn to the angle-differential photoionization cross section.

For two-photon ionization of a target atom by linearly polarized light, the angle-differential photoionization cross section is given by

$$\frac{d\sigma}{d\Omega} = \frac{\sigma_0}{4\pi}[1 + \beta_2 P_2(\cos\theta) + \beta_4 P_4(\cos\theta)], \qquad (4)$$

where σ_0 is the total photoionization cross section, θ is the angle between the photoelectron momentum vector and the polarization vector of the light, β_2 and β_4 are the second- and fourth-order anisotropy parameters, and P_2 and P_4 are the second- and fourth-order Legendre polynomials in variable $\cos\theta$ [34]. The measured angle-differential photoionization amplitude is presented in Fig. 3. Equation (4) has been applied to fit the data (solid red line) using the projection method discussed in Ref. [35] where the error on the β parameters is determined via statistical bootstrapping [36]. The β parameters retrieved from the fit are $\beta_2 = -0.93 \pm 0.02$, $\beta_4 = 0.25 \pm 0.03$.

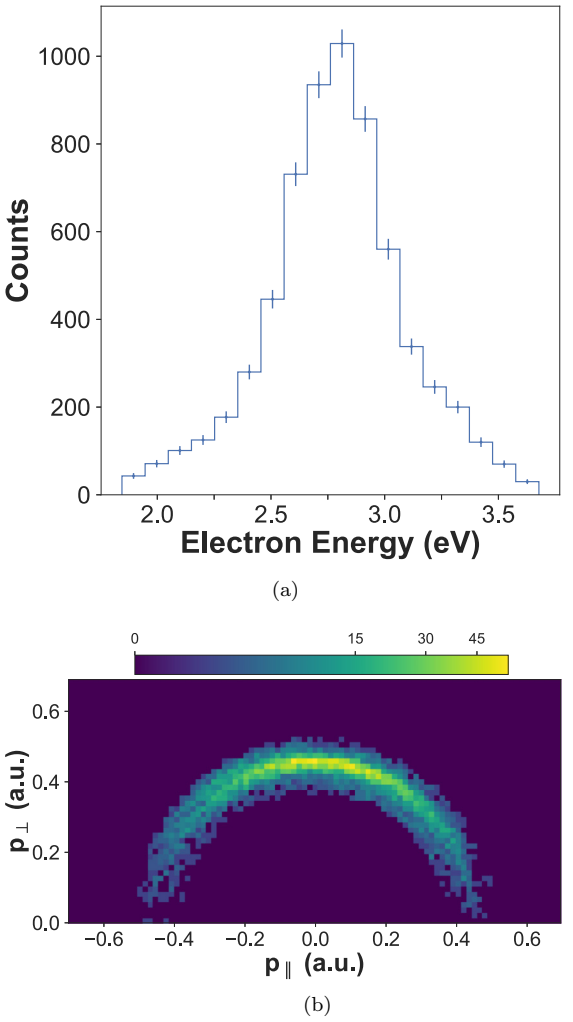

FIG. 2. (a) The photoelectron energy spectrum and (b) momentum distribution parallel versus perpendicular to the VUV polarization.

The PAD exhibits peak intensity at angles near $\pi/2$, corresponding with maximum photoelectron emission perpendicular to the VUV polarization. Intensity minima occur along the VUV polarization direction, near 0 and π. We attribute these features to the interference between the different p- and f-wave components of the photoelectron scattering wave function. These two angular momentum components destructively interfere along the polarization direction, yielding an angle-differential amplitude that peaks perpendicular to the field. This interference is analogous to the interference between the photoelectron s and the d partial waves in photodetachment of I^- and O^- [37–39].

We compare our retrieved β parameters with those extracted from Ref. [21] at a photon energy of 9.3 eV and Ref. [22] at a photon energy of 8.6 eV, presented in Table I and Fig. 4. In Ref. [21], the calculations were performed using a second-order time-independent perturbation theory method in both a Hartree-Fock (HF) approach and a Coulomb correlated HF approach. In the uncorrelated HF calculation, there is significant disagreement between the length and the velocity gauges, whereas the Coulomb correlated HF approach

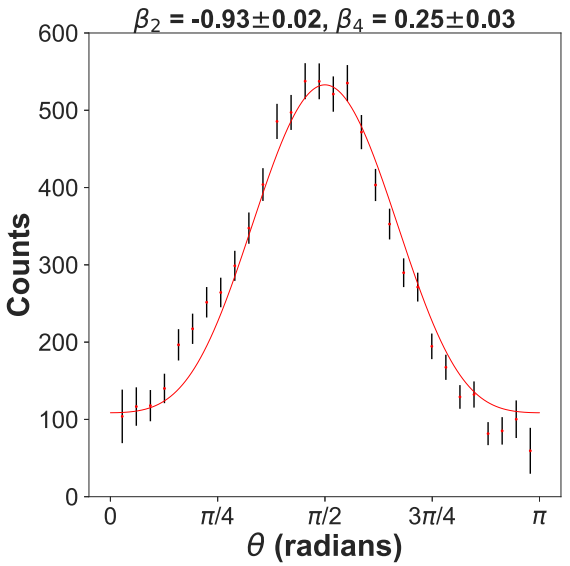

FIG. 3. The angle-differential photoionization cross section for NOTPSI of Ar at 9.3 eV. The experimental data are fit using Eq. (4) where the retrieved β parameters are displayed above the plot.

exhibits much better gauge invariance. We find that the Coulomb correlated HF calculations show good qualitative agreement with the present measurements [seen in Fig. 4(b)], specifically in the direction of maximum photoelectron emission. There are, however, significant quantitative discrepancies in the magnitude of β_2 and the sign of β_4 (see Table I). The uncorrelated HF calculations of Ref. [21] in either the length or the velocity gauge compare less favorably with the present measurements [seen in Fig. 4(a)].

In Ref. [22], the two-photon ionization cross sections were calculated using a random-phase-approximation method with HF wave functions for the initial, intermediate, and target states, neglecting electron-electron correlation. There is reasonable agreement at this photon energy between the calculations in length and velocity gauge [seen in Fig. 4(c)]. They both resemble the uncorrelated results in the velocity gauge of Ref. [21] shown in Fig. 4(a). However, there is poor qualitative and quantitative agreements between the uncorrelated theories and the measurement. Despite the quantitative disagreements, the correlated HF results of Ref. [21] suggest that electron-

TABLE I. The β parameters extracted from the calculations in Ref. [21] at a photon energy of 9.3 eV, in Ref. [22] at a photon energy of 8.6 eV, and those retrieved from the present measurement.

	β_2	β_4
HF length [21]	−0.62	−0.18
HF velocity [21]	−0.13	−0.48
Correlated length [21]	−0.54	−0.05
Correlated velocity [21]	−0.48	−0.01
Random-phase approximation length [22]	0.03	−0.62
Random-phase approximation velocity [22]	0.04	−0.58
Experiment	−0.93	0.25

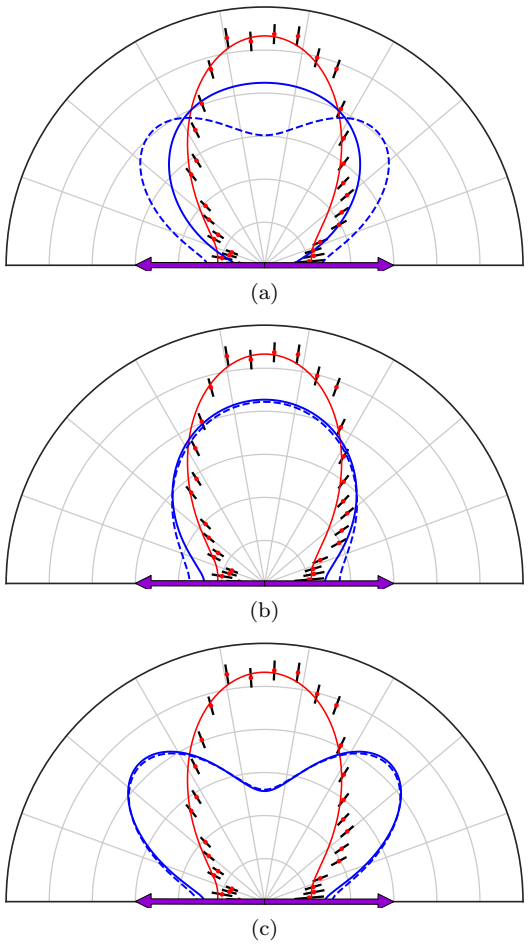

FIG. 4. The photoelectron angular distribution for NOTPSI of Ar at 9.3 eV for the experimentally retrieved β parameters [solid red curve in (a)–(c)] and those extracted from Refs. [21,22]. The blue curves in (a) correspond with the uncorrelated HF calculation of Ref. [21], the blue curves in (b) correspond with the Coulomb correlated calculation of Ref. [21], and the blue curves in (c) correspond with the random-phase-approximation calculation of Ref. [22] (dashed curve: velocity gauge; solid curve: length gauge). The orientation, the VUV polarization, is indicated by the horizontal double arrows.

electron correlation is essential in the accurate description of the NOTPSI dynamics of argon.

The discrepancies between the theory in Refs. [21,22] and the present measurements may be attributed to an inadequate treatment of electron-electron correlation in the calculations. The level of correlation accounted for in the Coulomb correlated HF approach of Ref. [21] led to better gauge invariance and a PAD with greater similarity to the present measurements. This suggests that a higher level of electron-electron correlation must be included for a more accurate description of NOTPSI in argon.

In conclusion, we have reported results on NOTPSI of argon using 3D momentum imaging and an intense 9.3-eV fs pulse. We find that the observed photoelectron emission pattern can be explained by the interference between the different p- and f-partial-wave components of the photoelectron scattering wave function, which add destructively

along the polarization direction of the ionizing VUV field. Our measurements are compared against a previous set of calculations, which reveal that the photoionization dynamics are evidently influenced by electron-electron correlation effects. It appears that the level of electron-electron correlation accounted for in the Coulomb correlated HF calculations in Ref. [21] is not sufficient to reach complete agreement with the present results. Our measurements can serve as a benchmark for future *ab initio* theoretical treatments of NOTPSI dynamics in multielectron systems. A particular challenge may be incorporating continuum-continuum coupling in the calculations, which is expected to be important in reproducing the PAD in nonresonant regions [40]. In addition to further the development of theoretical methods, there is a clear need for follow-up experiments to investigate the photon energy dependence of electron-electron correlation effects by angle-resolved photoionization of multielectron atoms and small molecules using intense VUV, XUV, and soft x rays, preferably at photon energies where calculated anisotropy parameters are gauge invariant, and correlated and uncorrelated results differ markedly.

Work at Lawrence Berkeley National Laboratory was performed under the auspices of the U.S. Department of Energy under Contract No. DE-AC02-05CH11231 and was supported by the U.S. Department of Energy Office of Basic Energy Sciences, Division of Chemical Sciences, Biosciences and Geosciences. This research used resources of the National Energy Research Scientific Computing Center (NERSC), a U.S. Department of Energy Office of Science User Facilities under Contract No. DE-AC02-05CH11231. We are indebted to the RoentDek Company for long-term support with detector software and hardware. We thank R. Y. Bello, R. R. Lucchese, and C. W. McCurdy for the many helpful discussions.

[1] D. I. R. Boll, O. A. Fojón, C. W. McCurdy, and A. Palacios, Angularly resolved two-photon above-threshold ionization of helium, Phys. Rev. A **99**, 023416 (2019).

[2] F. L. Yip, T. N. Rescigno, C. W. McCurdy, and F. Martín, Fully Differential Single-Photon Double Ionization of Neon and Argon, Phys. Rev. Lett. **110**, 173001 (2013).

[3] R. R. Lucchese, Effects of interchannel coupling on the photoionization cross sections of carbon dioxide, J. Chem. Phys. **92**, 4203 (1990).

[4] B. Basden and R. R. Lucchese, Vibrationally resolved cross sections and asymmetry parameters for the photoionization of n_2 with coupling between the $(3\sigma_g)^{-1}$ and the $(2\sigma_u)^{-1}$ channels, Phys. Rev. A **37**, 89 (1988).

[5] J. Jose, R. R. Lucchese, and T. N. Rescigno, Interchannel coupling effects in the valence photoionization of SF_6, J. Chem. Phys. **140**, 204305 (2014).

[6] R. E. Stratmann and R. R. Lucchese, Resonances and the effects of interchannel coupling in the photoionization of CS_2, J. Chem. Phys. **97**, 6384 (1992).

[7] T. N. Rescigno, B. H. Lengsfield, and A. E. Orel, Interchannel coupling and ground state correlation effects in the photoionization of CO, J. Chem. Phys. **99**, 5097 (1993).

[8] R. G. Houlgate, K. Codling, G. V. Marr, and J. B. West, Angular distribution and photoionization cross section measurements on the 3p and 3s subshells of argon, J. Phys. B: At. Mol. Phys. **7**, L470 (1974).

[9] Z. Altun and S. T. Manson, Photoelectron angular distributions of ns subshells of open-shell atoms as indicators of interchannel coupling: Sc $4s$ photoionization, Phys. Rev. A **61**, 030702 (2000).

[10] S. H. Southworth, A. C. Parr, J. E. Hardis, and J. L. Dehmer, Channel coupling and shape resonance effects in the photoelectron angular distributions of the $3\sigma_g^{-1}$ and $2\sigma_u^{-1}$ channels of N_2, Phys. Rev. A **33**, 1020 (1986).

[11] C. D. Lin, Channel interaction and threshold behavior of photoionization, Phys. Rev. A **9**, 171 (1974).

[12] D. J. Kennedy and S. T. Manson, Photoionization of the noble gases: Cross sections and angular distributions, Phys. Rev. A **5**, 227 (1972).

[13] L. H. Haber, B. Doughty, and S. R. Leone, Photoelectron angular distributions and cross section ratios of two-color two-photon above-threshold ionization of argon, J. Phys. Chem. A **113**, 13152 (2009).

[14] S. Mondal, H. Fukuzawa, K. Motomura, T. Tachibana, K. Nagaya, T. Sakai, K. Matsunami, S. Yase, M. Yao, S. Wada, H. Hayashita, N. Saito, C. Callegari, K. C. Prince, C. Miron, M. Nagasono, T. Togashi, M. Yabashi, K. L. Ishikawa, A. K. Kazansky, N. M. Kabachnik, and K. Ueda, Pulse-delay effects in the angular distribution of near-threshold EUV + IR two-photon ionization of Ne, Phys. Rev. A **89**, 013415 (2014).

[15] S. Düsterer, G. Hartmann, C. Bomme, R. Boll, J. T. Costello, B. Erk, A. De Fanis, M. Ilchen, P. Johnsson, T. J. Kelly *et al.*, Two-color XUV + NIR femtosecond photoionization of neon in the near-threshold region, New J. Phys. **21**, 063034 (2019).

[16] N. Miyamoto, M. Kamei, D. Yoshitomi, T. Kanai, T. Sekikawa, T. Nakajima, and S. Watanabe, Observation of Two-Photon Above-Threshold Ionization of Rare Gases by XUV Harmonic Photons, Phys. Rev. Lett. **93**, 083903 (2004).

[17] T. Sekikawa, A. Kosuge, T. Kanai, and S. Watanabe, Nonlinear optics in the extreme ultraviolet, Nature (London) **432**, 605 (2004).

[18] T. Sato, A. Iwasaki, K. Ishibashi, T. Okino, K. Yamanouchi, J. Adachi, A. Yagishita, H. Yazawa, F. Kannari, M. Aoyma *et al.*, Determination of the absolute two-photon ionization cross section of he by an XUV free electron laser, J. Phys. B: At., Mol. Opt. Phys. **44**, 161001 (2011).

[19] M. Meyer, D. Cubaynes, V. Richardson, J. T. Costello, P. Radcliffe, W. B. Li, S. Düsterer, S. Fritzsche, A. Mihelic, K. G. Papamihail, and P. Lambropoulos, Two-Photon Excitation and Relaxation of the $3d-4d$ Resonance in Atomic Kr, Phys. Rev. Lett. **104**, 213001 (2010).

[20] R. Ma, K. Motomura, K. L. Ishikawa, S. Mondal, H. Fukuzawa, A. Yamada, K. Ueda, K. Nagaya, S. Yase, Y. Mizoguchi *et al.*, Photoelectron angular distributions for the two-photon ionization of helium by ultrashort extreme ultraviolet free-electron laser pulses, J. Phys. B: At., Mol. Opt. Phys. **46**, 164018 (2013).

[21] C. Pan and A. F. Starace, Angular distribution of electrons following two-photon ionization of the Ar atom and two-photon detachment of the F^- ion, Phys. Rev. A **44**, 324 (1991).

[22] R. Moccia, N. K. Rahman, and A. Rizzo, Two-photon ionisation cross section calculations of noble gases: Results for Ne and Ar, J. Phys. B: At. Mol. Phys. **16**, 2737 (1983).

[23] R. Dörner, V. Mergel, O. Jagutzki, L. Spielberger, J. Ullrich, R. Moshammer, and H. Schmidt-Böcking, Cold target recoil ion momentum spectroscopy: A 'momentum microscope' to view atomic collision dynamics, Phys. Rep. **330**, 95 (2000).

[24] J. Ullrich, R. Moshammer, A. Dorn, R. Dörner, L. Ph. H. Schmidt, and H. Schmidt-Böcking, Recoil-ion and electron momentum spectroscopy: Reaction-microscopes, Rep. Prog. Phys. **66**, 1463 (2003).

[25] T. Jahnke, T. Weber, T. Osipov, A. L. Landers, O. Jagutzki, L. P. H. Schmidt, C. L. Cocke, M. H. Prior, H. Schmidt-Böcking, and R. Dörner, Multicoincidence studies of photo and auger electrons from fixed-in-space molecules using the coltrims technique, J. Electron Spectrosc. Relat. Phenom. **141**, 229 (2004).

[26] F. P. Sturm, T. W. Wright, D. Ray, I. Zalyubovskaya, N. Shivaram, D. S. Slaughter, P. Ranitovic, A. Belkacem, and T. Weber, Time resolved 3d momentum imaging of ultrafast dynamics by coherent VUV-XUV radiation, Rev. Sci. Instrum. **87**, 063110 (2016).

[27] Roentdek, Roentdek delayline detectors, http://www.roentdek.com.

[28] O. Jagutzki, A. Cerezo, A. Czasch, R. Dorner, M. Hattas, M. Huang, V. Mergel, U. Spillmann, K. Ullmann-Pfleger, T. Weber *et al.*, Multiple hit readout of a microchannel plate detector with a three-layer delay-line anode, IEEE Trans. Nucl. Sci. **49**, 2477 (2002).

[29] T. K. Allison, J. van Tilborg, T. W. Wright, M. P. Hertlein, R. W. Falcone, and A. Belkacem, Separation of high order harmonics with fluoride windows, Opt. Express **17**, 8941 (2009).

[30] H. H. Li, Refractive index of alkaline earth halides and its wavelength and temperature derivatives, J. Phys. Chem. Ref. Data **9**, 161 (1980).

[31] T. Sekikawa, T. Katsura, S. Miura, and S. Watanabe, Measurement of the Intensity-Dependent Atomic Dipole Phase of a High Harmonic by Frequency-Resolved Optical Gating, Phys. Rev. Lett. **88**, 193902 (2002).

[32] T. Sekikawa, T. Ohno, T. Yamazaki, Y. Nabekawa, and S. Watanabe, Pulse Compression of a High-Order Harmonic by Compensating the Atomic Dipole Phase, Phys. Rev. Lett. **83**, 2564 (1999).

[33] K. A. Larsen, J. P. Cryan, N. Shivaram, E. G. Champenois, T. W. Wright, D. Ray, O. Kostko, M. Ahmed, A. Belkacem, and D. S. Slaughter, Vuv and xuv reflectance of optically coated mirrors for selection of high harmonics, Opt. Express **24**, 18209 (2016).

[34] K. L. Reid, Photoelectron angular distributions, Annu. Rev. Phys. Chem. **54**, 397 (2003).

[35] X.-J. Liu, R. R. Lucchese, A. N. Grum-Grzhimailo, Y. Morishita, N. Saito, G. Prümper, and K. Ueda, Molecular-frame photoelectron and electron-frame photoion angular distributions and their interrelation, J. Phys. B: At., Mol. Opt. Phys. **40**, 485 (2007).

[36] B. Efron, *Breakthroughs in Statistics* (Springer, Berlin, 1992), pp. 569–593.

[37] R. Mabbs, E. R. Grumbling, K. Pichugin, and A. Sanov, Photoelectron imaging: An experimental window into electronic structure, Chem. Soc. Rev. **38**, 2169 (2009).

[38] J. L. Hall and M. W. Siegel, Angular dependence of the laser photodetachment of the negative ions of carbon, oxygen, and hydrogen, J. Chem. Phys. **48**, 943 (1968).

[39] J. Cooper and R. N. Zare, Angular distribution of photoelectrons, J. Chem. Phys. **48**, 942 (1968).

[40] R. Y. Bello (private communication).